UCRL-TR-223183

FLASH X-RAY (FXR) LINEAR INDUCTION ACCELERATOR (LIA) OPTIMIZATION

Sensor Delay Correction

Mike M. Ong

Tim L. Houck

Blake R. Kreitzer

Robert D. Paris

George E. Vogtlin

Jan Mark Zentler

April 2006

Disclaimer

Auspices

This work was performed under the auspices of the U.S. Department of Energy by University of California, Lawrence Livermore National Laboratory under Contract W-7405-Eng-48.

Table of Contents

1 Summary

The radiographic goal of the FXR Optimization Project is to generate an x-ray pulse with peak energy of 19 MeV, spot-size of 1.5 mm, a dose of 500 rad, and duration of 60 ns. The electrical objectives are to generate a 3 kA electron-beam and refine our 16 MV accelerator so that the voltage does not vary more than 1%-rms.

In a multi-cell linear induction accelerator, like FXR, the timing of the acceleration pulses relative to the beam is critical. The pulses must be timed optimally so that a cell is at full voltage before the beam arrives and does not drop until the beam passes. In order to stay within the energy-variation budget, the synchronization between the cells and beam arrival must be controlled to a couple of nanoseconds. Therefore, temporal measurements must be accurate to a fraction of a nanosecond.

FXR Optimization Project developed a one-giga-sample per second (gs/s) data acquisition system to record beam sensor data. Signal processing algorithms were written to determine cell timing with an uncertainty of a fraction of a nanosecond. However, the uncertainty in the sensor delay was still a few nanoseconds. This error had to be reduced if we are to improve the quality of the electron beam.

Two types of sensors are used to align the cell voltage pulse against the beam current. The beam current is measured with resistive-wall sensors. The cell voltages are read with capacitive voltage monitors. Sensor delays can be traced to two mechanisms: (1) the sensors are not co-located at the beam and cell interaction points, and (2) the sensors have different length jumper cables and other components that connect them to the standard-length coaxial cables of the data acquisition system.

Using the physical locations and dimensions of the sensor components, and the dielectric constant of the materials, delay times were computed. Relative to the cell voltage, the beam current was theoretically reporting late by 7.7 ns. Two experiments were performed to verify and refine the sensor delay correction.

In the first experiment, the beam was allowed to drift through a cell that was not pulsed. The beam induces a potential into the cell that is read by the voltage monitor. Analysis of the data indicated that the beam sensor signal was likely 7.1 ns late.

In the second experiment, the beam current is calculated from the injector diode voltage that is the sum of the cell voltages. A 7 ns correction produced a very good match between the signals from the two types of sensors.

For simplicity, we selected a correction factor that advanced the current signals by 7 ns. This should reduce the uncertainty in the temporal measurements to less than 1 ns.

2 Introduction

This report describes LLNL's Flash X-ray (FXR) beam sensor delay corrections that are required to reduce timing measurement uncertainty to less than 1 ns. The corrections are developed theoretically, and verified and refined using data from two different experiments.

The radiographic goal of the FXR Optimization Project is to generate an x-ray pulse with peak energy of 19 MeV, spot-size of 1.5 mm, a dose of 500 rad, and duration of 60 ns. The electrical objectives are to generate a 3 kA electron-beam and refine our 16 MV accelerator so that the voltage does not vary more than 1%-rms.

In a multi-cell linear induction accelerator like FXR, the timing of the acceleration pulses relative to the beam is critical [1]. (See Figure 2.1.) The acceleration pulses must be timed optimally so that a cell is at full voltage before the beam arrives and does not drop until the beam passes.

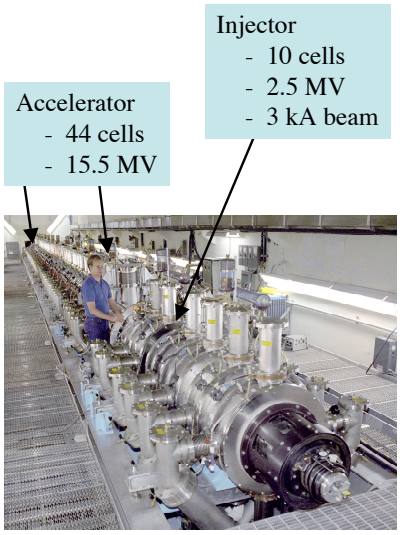

Figure 2.1. FXR is a multi-cell accelerator.

Because of timing jitter associated with more than a hundred high-voltage gas switches, the duration of the accelerator cell voltage flat-top must be 70 ns even though the electron beam is only effectively 60 ns long. With a simple model of the cell voltage that incorporates the rise- and fall-times and rounded corner features, the cell timing jitter and drift can be converted to beam energy-variation. In order to stay within the energy-variation budget, the synchronization between the cells and beam arrival must be controlled to a couple of nanoseconds. Therefore, temporal measurements must be accurate to a fraction of a nanosecond.

FXR needed a measurement system capable of making sub-nanosecond measurements. A couple of years ago, a new one giga-sample per second data acquisition system was developed to record beam sensor data. Signal processing algorithms were written to determine cell timing with an uncertainty of a fraction of a nanosecond. However, the uncertainty in the sensor delay was still a few nanoseconds. The Optimization Project wanted to reduce this error so we can improve the quality of the electron beam.

Many years ago the beam was temporally aligned with the cells by adding or cutting cables. The cables carried the trigger pulse to the high-voltage gas switches that started the pulse into the cell. While we still do this for relatively large timing errors of more than 5 ns, smaller corrections can now be made with the new SF6 gas system [2, 3]. The gas pressure in the switch determines the turn-on delay. We have the ability to set timing to an accuracy of better than a nanosecond. Wear and refurbishment on these switches produce delay changes. Therefore, periodic timing adjustments are needed.

The Sensors

FXR has a voltage monitor on every cell. (See Figure 2.2) The sensing element is a metal and dielectric disk that forms a capacitor inside the cell. This capacitor detects a small

portion of the electric-field in the cell. The signal is integrated by adding a resistor in series to the sensing capacitor. The resistor is inside the blue box in Figure 2.2. The standard-length Heliax coaxial cable from the data acquisition is attached to the end of the box. Therefore, everything between the disk and the coaxial cable adds a delay to the voltage signal.

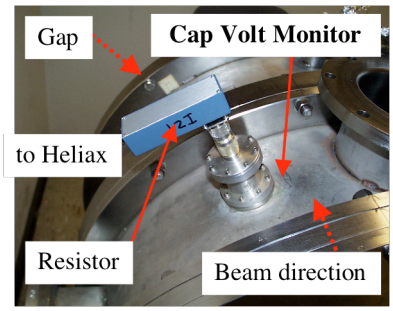

Figure 2.2. The cell voltage monitor is in the cell.

There is another "delay" associated with this sensor. The beam is accelerated when it crosses the gap of the cell. (See Figure 2.3.) Ideally the voltage monitor would be placed in the center of the beam-line so the sensor can report the electric field experienced by the beam. Of course, this is not practical. Instead, the voltage monitor is located near the pulse-power feed to the cell. Therefore, the voltage signal arrives early relative to the beam that is under the acceleration gap. The sensor is situated in the section of the cell that is filled with oil. Because the dielectric constant of oil is greater than one, the electromagnetic (EM) wave will travel slower than the speed of light. These two effects, location and speed difference, must be included in the timing correction.

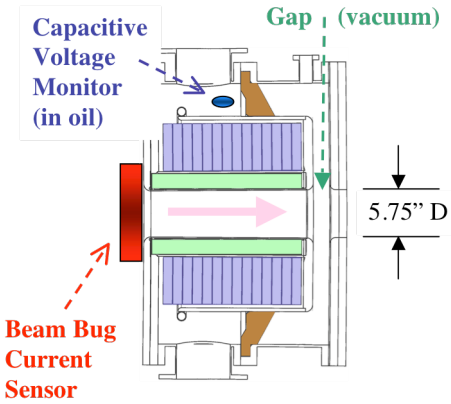

Figure 2.3. Location of the voltage and current sensors.

The beam current sensor, also known as a beam bug, is shown on the left side of Figure 2.3. Ideally, it would be placed under the gap where the action is. The beam enters the left side of the cell, and therefore the current signal is reported early. There is only one beam bug for each block that consists of four cells.

The beam bug assembly is shown in Figure 2.4. The sensing element is a resistive foil that is a part of the beam-line. The voltage is measured in four locations. The sum of these four signals produces the current level. The addition is done in the gold box on the right side of the figure. The gray boxes perform subtraction, and the difference indicates the position of the beam. The signals from the sensing ring to the boxes are carried on coaxial cables with a solid copper outer jacket for shielding, also known as CuJack. These delays will feed into the correction calculations.

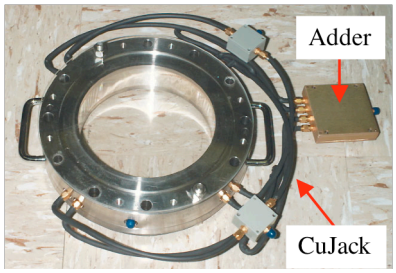

Figure 2.4. Beam current is measured with a beam bug.

The Data Acquisition System

The new high-speed digitizers shown in Figure 2.5 were purchased from Acqiris and are installed at four different locations along the beam-line. They are housed in four electromagnet interference (EMI) shielded boxes. The sample rate for the beam-bug and voltage monitor signals is one giga-sample per second.

The new data acquisition system has three features that mitigate or correct timing differences. (See Figure 2.6) (1) All of the data acquisition signal cables are of the same length. If ideal sensors were connected directly to these cables, without jumpers, timing corrections would be unnecessary. (2) The four digitizer chassis receive the record command at the same time because the cables from the trigger system are all of the same length. (3) Within a chassis, the trigger signal is distributed to the modules that contain up to four digitizers. The Acqiris system compensates for these small differences of less than one nanosecond. It adds timing corrections to the different channels based on the location of the module in the chassis. In summary, the timing differences in the new data acquisition system have been either mitigated or corrected in hardware. We only have to focus on correcting the sensor delays.

Figure 2.5. New FXR digitizers are protected by EMI boxes.

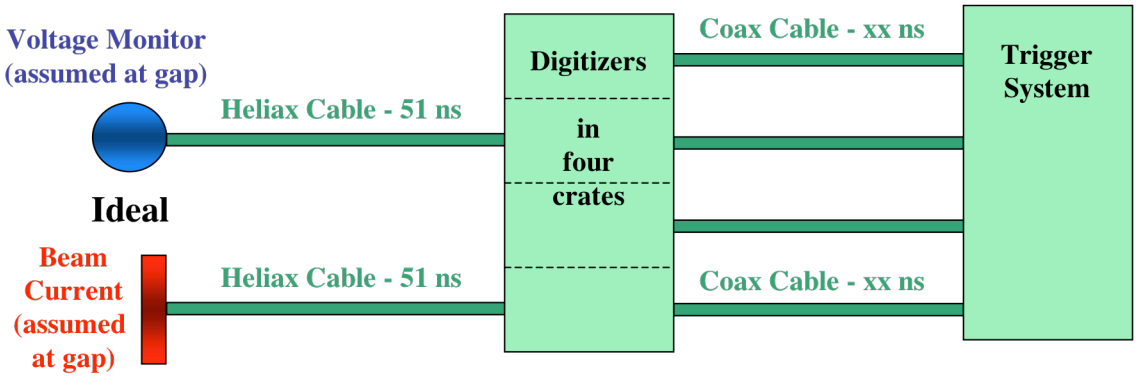

Figure 2.6. New FXR data acquisition corrects for timing differences between channels.

Two more concepts will be presented that will be helpful for understanding the timing problem and the sensor correction validation. (1) FXR is a distributed pulse-power machine with sensors collecting data along the beam-line. This data can be consolidated into a single plot if we remove the electron time-of-flight (TOF) effect. (2) The absolute timing of a cell is less important than the relative timing with respect to the beam.

The optimal and actual firing times of the injector and accelerator cells are shown in Figure 2.7. The two blue lines represent the time required for an electron traveling at the speed of light to move from one cell to the next. The injector cell timing, shaped like an inverted "V", is different from the accelerator timing because the electrons must travel from two directions. Electrons start from the far end of the cathode and anode and converge at the injector diode located at the peak of the inverted "V". On the accelerator line, the uneven spacing of the cells causes changes in the slope. The timing between the left injector blue line and the right accelerator line determines the alignment of the beam in the accelerator. The

bars indicate the actual cell timing for a particular shot. Timing jitters in the high-voltage switches and slower drifts from switch wear cause the timing errors.

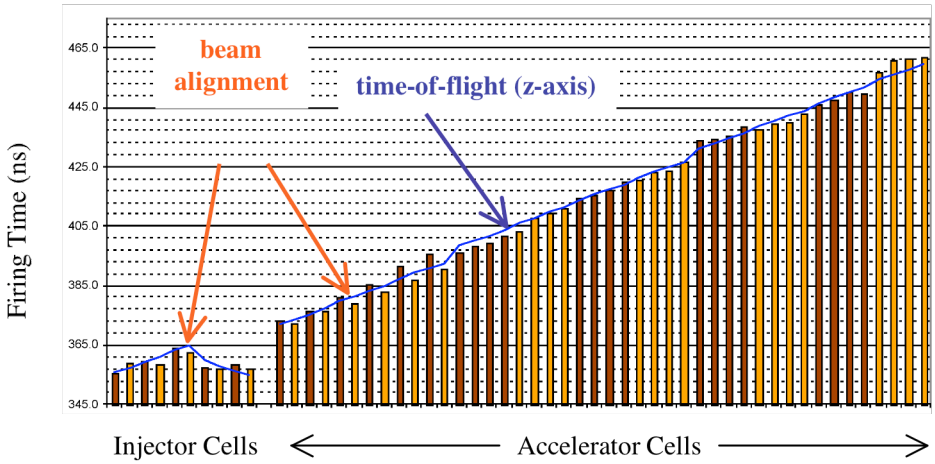

Figure 2.7. The beam time-of-flight to a cell determines cell firing time.

FXR data processing software can remove the time-of-flight effect on both cell voltage monitors and beam current sensor. The code has the location of all the sensors on the long axis of the machine, z-axis. The travel time between sensors is calculated by dividing the spacing by the speed of light. By removing the spatial considerations, the beam alignment can easily be checked at any cell. The voltages with time-of-flight adjustments from all the accelerator cells can also be added together to produce a total acceleration voltage, and the beam timing can be checked against this composite signal. Plots we will use in the rest of the report will use this feature; the time-of-flight effect is removed.

3 Sensor Delay Correction

While it may seem simple, derivation of the sensor delay correction can be very confusing. So a detailed and careful explanation will be given. We will examine the timing differences between an ideal set of sensors and the real FXR sensors.

The point of interest in an accelerator is the volume formed by the two vertical planes extending across the gap and the beam pipe. (See Figure 3.1) In this volume the beam (pink arrow) gains energy from the electrical field created by the pulse-power voltage (blue arrows) across the gap. An ideal set of sensors would be positioned at the intersection of the beam pipe center-line and center plane located in the middle of the gap.

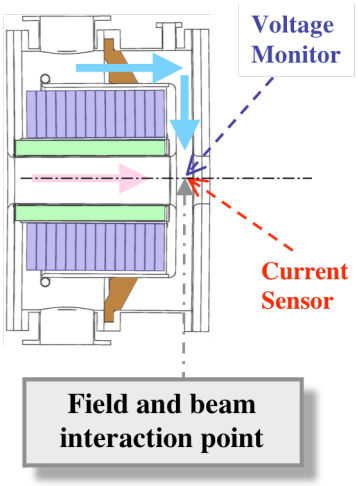

Figure 3.1. Ideal sensors would be located in the interaction point.

Figure 3.2 shows our perfect data acquisition system. The sensors instantaneously produce an output, without delay, and the equal length cables are directly attached to the sensor. In this configuration, only a time-of-flight correction is needed.

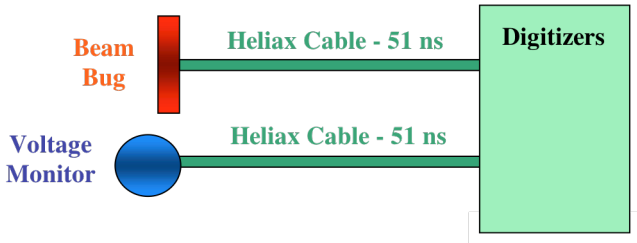

Figure 3.2. Ideal data acquisition has equal length sensor cables.

The cell voltage and beam current signals from our hypothetical measurement system are displayed in Figure 3.3. The data is not real and was generated to illustrate a typical temporal relationship between the cell voltage and beam current. The cell voltage comes up to almost full voltage before the beam arrives. Let's get real.

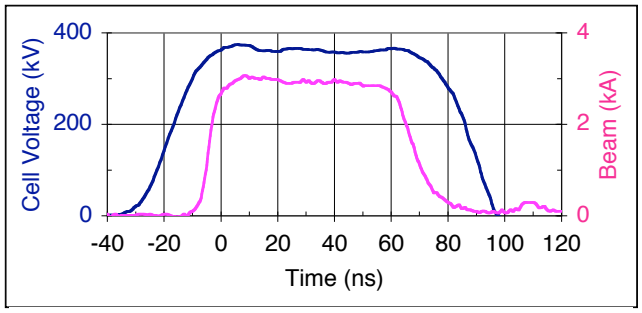

Figure 3.3. Display of ideal sensor data.
for illustration only - not real data

Current Sensor

We will describe a real current sensor first and then analyze the voltage monitor. On FXR, the beam bugs are mounted on the upstream side of the cells. They sense the beam before it enters the gap region. The time-of-flight software assumes the voltage monitor is in the ideal location and the beam bug is on the left side of a cell block. We need to develop an additional correction to account for the real sensors. We will concentrate on the delays created by the sensor, cable to adder, adder and jumper to the standard-length data acquisition cables. (See back to Figure 2.4.)

These different delays can be lumped together and represented by a jumper cable added between the ideal sensor and the ideal data acquisition system. (See Figure 3.4.) The resulting delayed current is shown in red in Figure 3.5 and is shifted to the right of the ideal signal denoted in pink. The delay was arbitrarily chosen to be 5 ns.

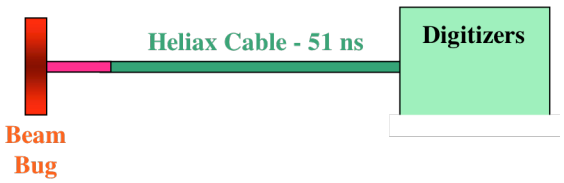

Figure 3.4. Delays associated with a real beam-bug can be represented as a jumper.

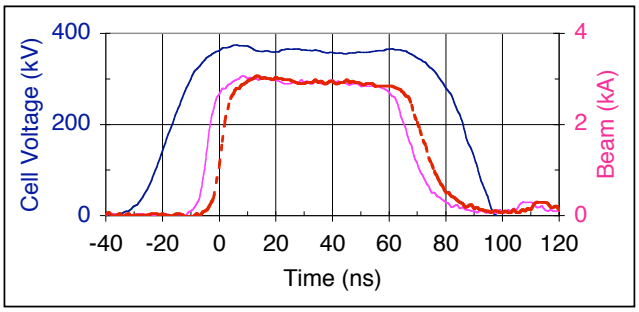

Figure 3.5. Display of delayed and ideal current sensor data.
for illustration only - not real data

Voltage Monitor

The voltage monitor timing is a little more difficult to conceptualize. The time-of-flight software assumes that the monitor is in the plane of the gap. We could not simply specify the actual location of the monitor on the z-axis because it also has a radial offset. (See Figure 3.6.) We chose to leave the time-of-flight data pointing to the gap location, and the sensor delay will include the timing to the actual sensor position. Analyzing the delay is more complex because the accelerating pulse is sensed before it arrives at the gap.

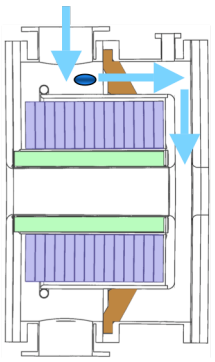

Figure 3.6. Voltage monitor is before the gap.

A way to conceptualize the problem is to pretend that the sensor is in the beam-line, and the standard-length cable is routed up the gap, back to the monitor position and out the hold where the sensor cable would come through. Now move the sensor to the actual location. The voltage signal is advanced by the time an electron travels in this piece of hypothetical cable. (See Figure 3.7.) The voltage monitor also has a delay element, like the current sensor, because of the connectors and resistor box. For illustration purposes, the combined effect is arbitrarily set at 5 ns early. The advanced signal shown in light blue in the plot in Figure 3.8 is to the left of the signal in blue from the ideal voltage sensor.

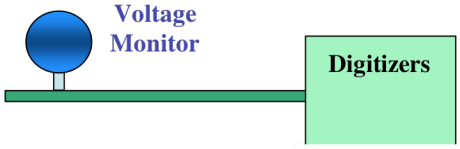

Figure 3.7. Voltage signal is advanced because of the sensor location.

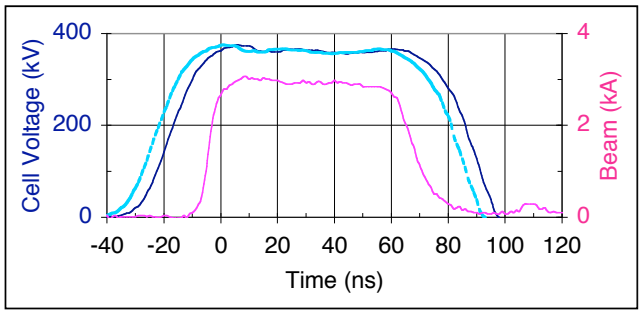

Figure 3.8. Display of advanced and ideal voltage monitor data.
for illustration only - not real data

Sensor Delay Correction

The total theoretical delay (T_{total}) will be derived by adding together the delays in each component and keeping track of the signs. The time delay in each component (t_i) depends on its length (l_i), the relative dielectric constant, (ε_i), and the propagation speed of light (c).

$$T_{total} = T_{beam-bug} - T_{volt-monitor} = \sum_{n} T_{beam-bug-i} - \sum_{n} T_{volt-monitor-i}$$

$$T_i = \frac{l_i}{v_i} = \frac{l_i}{c/\sqrt{\varepsilon_i}}$$

Propagation speed in a component is calculated by dividing the speed of light (c = 3.00 10^8 m/s = 11.80 in/ns) by the square root of the relative dielectric constant. The electron velocity in the beam (v) can be determined from the following equations:

$$\gamma_{injector} = \frac{E_{injector}}{E_0} = \frac{2.5 + 0.51\ \text{MeV}}{0.51\ \text{MeV}} = 6.1$$

$$\gamma_{FXR} = \frac{E_{FXR}}{E_0} = \frac{17.5 + 0.51\ \text{MeV}}{0.51\ \text{MeV}} = 34$$

$$\gamma_i = \frac{1}{\sqrt{1 - \frac{v_i^2}{c}}}$$

$$v_{injector} = 0.987c = 11.64\ \text{in/ns}\ ,\ v_{FXR} = 0.9996c = 11.80\ \text{in/ns}$$

The Lorentz factor (γ) is the ratio of the total electron energy divided by the rest energy (0.51 MeV). From the Lorentz factor, we can calculate the velocity of the electrons as a fraction of c. The slowest electrons are at the 2.5 MeV injector and are moving at 98.7% of c. The distance from the first accelerator cell to the next is 19.9 inches. The beam is 23 ps slower crossing this distance between the first and second accelerator cells than a light photon.

The electrons at the end of the 17.5 MeV accelerator are moving at 99.96% of c. Because the FXR gamma is large, the velocity of an electron in a cell can be estimated by a simplified equation:

$$v_{cell-i} \approx \left(1 - \frac{1}{2}\,\gamma_{cell-i}^{-2}\right) c$$

The inter-cell transit time between an electron and light photon is less than 1 ps. An electron starting at the velvet takes 0.2 ns longer than a light photo to reach the end of the accelerator. This slight slow down will be used in our first validation experiment. These timing differences are very small. For beam timing alignment where requirements are looser, we will simply use c for the velocity.

Calculating the velocity of the pulse-power wave in the cell is tedious because of the different components: oil, epoxy, and vacuum. (See Figure 3.7.) The relative dielectric constants and the propagation speeds are listed in Table 3.1. The relative dielectric constant of the epoxy is an estimate. The cables are assumed to have Teflon insulators. We could not find the dielectric constant or the delay for the adder box in the current signal path. We could have used a Time Domain Reflectometry (TDR) measurement. Given its small size, using typical cable velocities seem good enough.

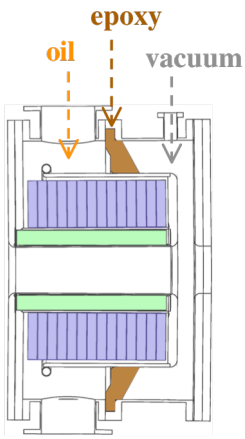

Figure 3.7. Cell has many types of materials.

Component	ε_r	Velocity
Vacuum	1	11.8 in/ns
Cell - oil	2.26	7.85 in/ns
Cell - epoxy	3.5	6.3 in.ns
Cable - Teflon	2.2	7.96 in/ns

Table 3.1. Cell has many relative dielectric constants and velocities.

Starting with the voltage monitor, the component or path delays for the two sensors are listed in Table 3.2. The resistor box and connectors are 11 inches long, and the delay is 0.93ns. The path from the voltage monitor to the gap does not create a delay, but an advance. The vacuum path in the cell is 18 inches. The distance from the gap to the center of the beam-line is also an advance. The total voltage monitor delay is -1.8 ns. This means the signal arrives earlier than expected at the standard-length data acquisition cable. The voltage signal correction is 1.8 ns delay.

The beam bug delays are real delays. The distance from the beam-bug resistive wall, or foil, to the connector was estimated to be 1 inch. The jumper cables are high-frequency components that will operate at more than 1 GHz. Therefore, we assumed that the insulator was Teflon. The delay in the beam bug was 5.9 ns.

The total delay for both sensors is 7.7 ns. (See Figure 3.8.) Another view of the problem is that the two sensors cause the ideal waveforms to be spread apart 7.7 ns. There are a number of remedies.

Component or Path	Delay	Note
Heliax to Volt Monitor	+0.93 ns	con'tor + Ω box ≈ 11"
Volt Monitor to Gap	-2.51 ns	oil ≈ 4", ins. ≈ 3", 18"
Gap to Beam-pipe CL	-0.24 ns	distance = 2.875 in.
Volt Mon'r sub-total	**- 1.8 ns**	shift plot later
Beam-pipe CL to BB	+0.24 ns	distance = 2.875 in.
Beam Bug internal	+0.08 ns	Guess 1 inch
BB to Adder Cable	+1.57 ns	13", cujak, v ≈ 0.7c?
Adder	+0.50 ns	ZFR4SC, ≈ 4", 0.7c?
Adder to Heliax Cable	+3.51 ns	29", flex, v ≈ .7c?
Beam Bug sub-total	**+ 5.9 ns**	shift plot early
Total Delay	**7.7 ns**	= | VM | + | BB |

Table 3.2. Beam bug and voltage monitor delays add up to 7.7 ns.

The delay correction can be applied to both types of sensors. All the sensors could be corrected. However, we chose the simplest solution: only advance the beam bugs because there are fewer of them. All of the beam bugs on the accelerator generate the same signal because there is no current lost along the beam-pipe. We suggest one more simplification. All the cell timings can be checked against just the first beam current sensor, I35, which is right after the injector.

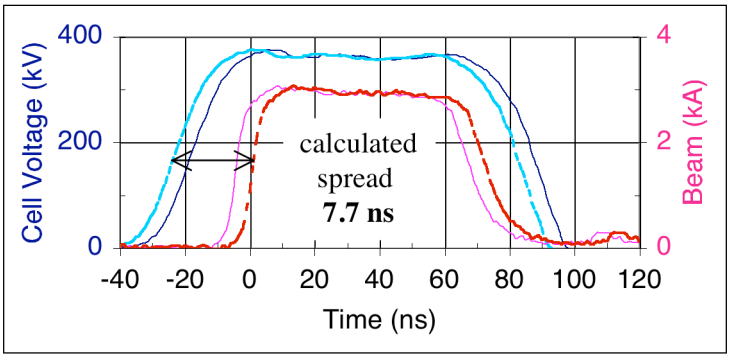

Figure 3.8. The sensor delays cause the signals to spread out an additional 7.7 ns.
for illustration only - not real data

- Only the beam current sensors will be advanced.
- Use beam bug I35 to check all the cell timings.

4 Delay Correction Validation

Two experiments were performed to verify and refine the sensor delay correction. In the first experiment, the beam was allowed to drift through a cell that was not pulsed. The beam induces a potential into the cell that was read by the voltage monitor. In the second experiment, the beam current is calculated from the injector diode voltage that is the sum of the cell voltages. Comparing the results will confirm our selection of a sensor delay correction time.

Beam-induced Cell Voltage Experiment

The beam-induced experiment was planned to verify the timing between the first beam current sensor and one of the later cell voltage monitors. On shot 150 574, the L Section pulse-power system was not turned on. The beam was allowed to pass through the section, and a cell voltage was analyzed. Since the beam was not gaining energy in L Section, the normal beam transport would eventually fail causing beam loss. Therefore, one of the first cells, L14, was analyzed.

The first step was to review the time-of-flight correction. Table 4.1 lists the time from the first cell (I11) in the injector to beam bug I35 at the end of the injector, and the TOF for voltage monitors in cells L13 and L14. The timing difference between these two cells converts to a separation of 19.90 inches, which matches the physical separation.

Sensor	TOF (ns) - Paris	To next sensor (ns)	Distance to next sensor
BB-I35	22.60		
VM-L13	86.76	1.68	19.90 in
VM-L14	88.76		

Table 4.1. Time-of-flight correction was checked against physical dimensions.

In this experiment, we need to repeat the sensor delay calculations with a twist. The total beam bug delay of 5.9 ns is unchanged from Table 3.2.

Component or Path	Delay	Note
Beam-pipe CL to BB	0.24 ns	distance = 2.875 in.
Beam Bug internal	0.08 ns	guess 1 inch
BB to Adder Cable	1.57 ns	13", cujak, v ≈ 0.7c?
Adder	0.50 ns	ZFR4SC, ≈ 4", 0.7c?
Adder to Heliax Cable	3.51 ns	29", flex, v≈ .7c?
Beam Bug sub-total	**5.9 ns**	
Beam Bug to Volt Mon	0.2 ns	relativistic correction
Beam-pipe CL to Gap	0.24 ns	distance = 2.875 in.
Gap to Volt Monitor	2.51 ns	oil ≈ 4", ins. ≈ 3", 18"
Volt Monitor to Heliax	0.93 ns	con'tor + Ω box ≈ 11"
Volt Mon'r sub-total	**3.9 ns**	
Difference	**2.0 ns**	VM data arrives first

Table 4.2. Calculated sensor delays show that the voltage monitor will report first.

The time-of-flight software based on the photon speed, c, compensates for the separation between beam bug I35 and voltage monitor L14. However, the relativistic mass of the electron adds 0.2 ns to the flight time.

The cell voltage delay calculation is different

because the EM waves are traveling in different directions. The voltage starts at the center of the beam-line and moves up into the cell monitor. The magnitude of delays are the same, but they are additive. The total voltage monitor delay is 3.9 ns. Therefore it will report 2.0 ns before the beam bug.

The data from the experiment is shown in Figure 4.1. As predicted, the voltage monitor (in blue) reports first. As expected the polarity of the pulse changed. The beam loading waveform should have the opposite potential as the accelerating pulse. The voltage signal is very small; the induced voltage is only about 6% of the pulse-power voltage. Therefore the signal was very weak and the noise was relatively high. To improve the signal-to-noise ratio, a 3-point running-average filter was applied.

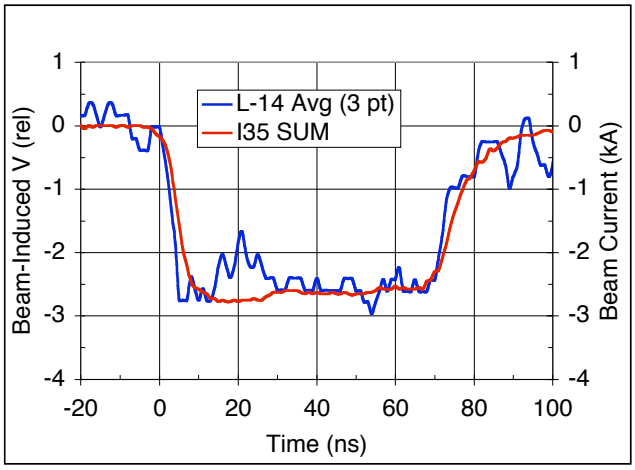

Figure 4.1. The induced cell voltage leads the beam bug current.

There are many more features on the induced voltage than the current measurement because of the reflecting electromagnetic waves created by impedance mismatches in the cell. The frequency responses of the two sensors are also different.

The timing difference between the two signals measured at 50% of maximum amplitude points is 1.4 ns. (See Figure 4.3.) The uncertainty is about ± 0.2 ns. The calculated delays based on physical dimensions predicted that the induced voltage signal would lead by 2.0 ns. So there is a 0.6 ns discrepancy.

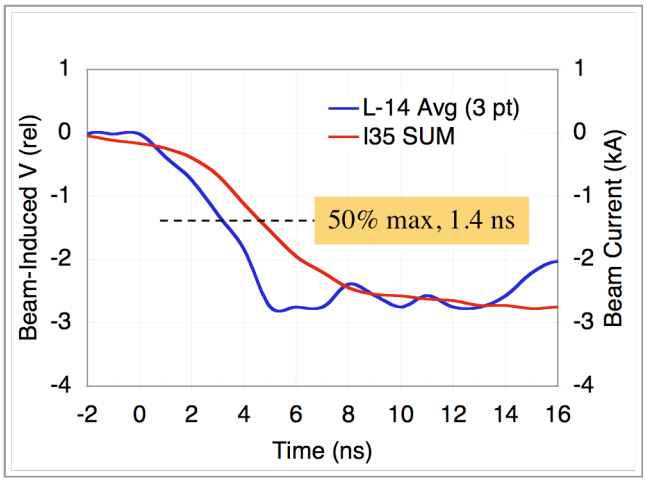

Figure 4.2. Lead edge of the beam bug signal follows the induced cell voltage.

Assuming the experimental data is correct, the calculated beam bug delay was either slightly too long and/or the voltage monitor was slightly too short. The voltage monitor delays cannot be made shorter without exceeding the speed of light. However, the uncertainty in the current sensing components is larger, and the delays could be longer. Using this argument, the experimental results suggest that the current delay is probably 6.5 ns rather than 5.9 ns. The spread should be 7.1 ns, or the current measure should be advanced by 7.1 ns rather than 7.7 ns.

The average of the computed and experimental delays is 7.4 ns. Our sample rate is 1 gs/s. To shift the data a fraction of a nanosecond requires transforming the data into the

frequency domain, and adding a linear phase term. The small improvement in temporal accuracy does not justify the computational cost.

For simplicity we will advance the current sensor data by 7 ns. The time shifting algorithm is very simple and quick. The uncertainty should be small enough so it will have minimal impact on beam energy-variation. In the remainder of this section, we will show the application and verification of this delay, 7 ns, on injector data.

Injector Current and Voltage Comparison

The data from the injector cell voltage monitors can be converted to beam current. By comparing the computed and measured current, we can determine if the selected correction time is appropriate.

The diode voltage can be estimated by summing the cell voltages with time-of-flight adjustments. The sum of the injector cells and the time-advanced beam current is shown in Figure 4.1.

To the first order, the beam current can be calculated from the injector diode voltage using the following equation:

$$i_{beam} = \mathrm{k}\ V_{diode}^{2/3}$$

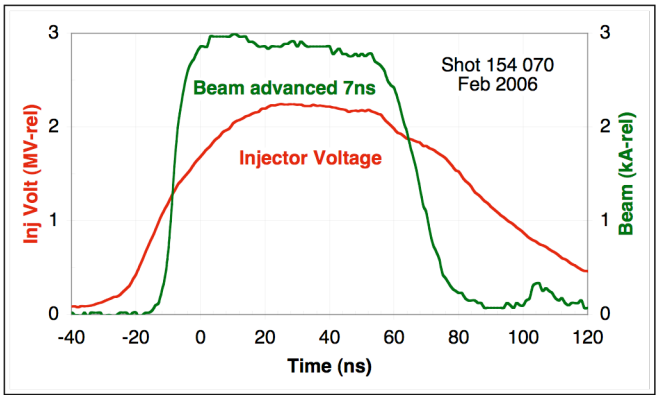

Figure 4.1. Beam current is advanced 7 ns and injector voltage is estimated from cell data.

The computed and measured time-advanced beam currents are shown in Figure 4.2. There is excellent agreement for the last 40 ns of the beam. The conformity is poor for the first 20 ns because the injector has a complex structure with cathode and anode stalks. At the beginning of the injector pulse, the electromagnetic waves are reflecting off the ends of the stalks. This effect has been simulated with a computer circuit code, and the results are similar to the ones in the figure.

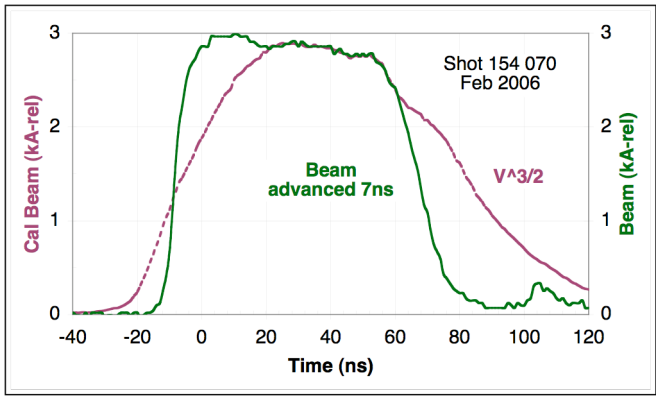

Figure 4.2. Advanced beam current and computed current match well for the last 40 ns.

Two refinements were considered, and both had little impact on this analysis. The electrons required additional time, 0.09 ns, to cross the cathode-anode gap of the injector when compared against a photon. (See Appendix.) The relativistic electrons also required another 0.1 ns to reach the I35 beam bug. Both effects would not be noticed in the above plot.

It appears that the 7 ns sensor delay correction time is very good.

Appendix – Injector Gap Transient Time

Tim Houck calculated the transit time for an electron to cross the cathode-anode gap on the FXR injector. His assumptions were: the electric field, E_z, is constant; the gap length, L, is 12 cm; and the injector voltage, V, is 2.1 MeV. The p is momentum; γ is the Lorentz term; m_0 is the rest mass of the electron; β is the ratio of the electron speed divided by c; and KE is the kinetic energy gained by an electron crossing the gap.

$$\frac{\partial p_z}{\partial t} = F_z = eE_z \approx e\frac{V}{L}$$

$$T = \int_o^T dt = \frac{L}{eV}\int_{p_i}^{p_f} dp_z = \frac{L}{eV}(p_f - p_i) = \frac{L\,p_f}{eV}$$

$$p_z = \gamma m_0 \beta c = m_0 c\sqrt{\gamma^2 - 1}$$

$$\gamma m_0 c^2 = KE + m_0 c^2 = eV + m_0 c^2$$

$$T_R = \left(\frac{L^2}{c^2} + \frac{2m_0 L^2}{eV}\right)^{1/2} = \frac{L}{c}\left(1 + \frac{2m_0 c^2}{eV}\right)^{1/2}$$

The transit time for a photon is simply L divided by c, or 0.40 ns. The relativistic effect adds another 0.09 ns. The relativistic transient time, T_r, for an electron is 0.49 ns.

Acknowledgements

We want to acknowledge Ed Koh for his computer support and Keith Lewis for keeping FXR running. We also wish to thank the rest of the Optimization Team for listening to the presentations and providing feedback that serve as the basis for this report. Lyn Ahboltin deserves credit for proofreading this document.

References

[1] Ong, Mike, et al, "FXR Linear Induction Accelerator (LIA) Optimization Energy Regulation Requirements and Upgrade Options, A System Approach, Part 1 of 2", August 2004, UCRL-TR209239, Lawrence Livermore National Laboratory.

[2] Ong, Mike, et al, "FXR Linear Induction Accelerator (LIA) Optimization Trigger Delay Requirements", December 2005, UCRL-TR-219445, Lawrence Livermore National Laboratory.

[3] Ross, Tim, "Sulfur Hexafluoride Distribution System for the Flash X-Ray (FXR) Facility Operating Procedure", March 2006, ERD500149-AA, Lawrence Livermore National Laboratory.

intentionally left blank